MDPI

*Article*

# Kinetic Modeling for the "One-Pot" Hydrogenolysis of Cellulose to Glycols over Ru@Fe$_3$O$_4$/Polymer Catalyst

Oleg Manaenkov [1,*] , Yuriy Kosivtsov [1], Valentin Sapunov [2] , Olga Kislitsa [1], Mikhail Sulman [1], Alexey Bykov [1], Alexander Sidorov [1] and Valentina Matveeva [1,3]

[1] Department of Biotechnology, Chemistry and Standardization, Tver State Technical University, 170026 Tver, Russia; kosivtsov@mail.ru (Y.K.); kislitza@yandex.ru (O.K.); science@science.tver.ru (M.S.); bykovav@yandex.ru (A.B.); sidorov_science@mail.ru (A.S.); valen-matveeva@yandex.ru (V.M.)
[2] Department of Chemical Technology of Basic Organic and Petrochemical Synthesis, Mendeleev University of Chemical Technology, 125047 Moscow, Russia; sapunovvals@gmail.com
[3] Regional Technology Center, Tver State University, 170100 Tver, Russia
* Correspondence: ovman@yandex.ru

**Abstract:** Despite numerous works devoted to the cellulose hydrogenolysis process, only some of them describe reaction kinetics. This is explained by the complexity of the process and the simultaneous behavior of different reactions. In this work, we present the results of the kinetic study of glucose hydrogenolysis into ethylene- and propylene glycols in the presence of Ru@Fe$_3$O$_4$/HPS catalyst as a part of the process of catalytic conversion of cellulose into glycols. The structure of the Ru-containing magnetically separable Ru@Fe$_3$O$_4$/HPS catalysts supported on the polymeric matrix of hypercrosslinked polystyrene was studied to propose the reaction scheme. As a result of this study, a formal description of the glucose hydrogenolysis process into glycols was performed. Based on the data obtained, the mathematical model of the glucose hydrogenolysis kinetics in the presence of Ru@Fe$_3$O$_4$/HPS was developed and the parameter estimation was carried out. The synthesized catalyst was found to be characterized by the enhanced magnetic properties and higher catalytic activity in comparison with previously developed catalytic systems (i.e., on the base of SiO$_2$). The summarized selectivity towards the glycols formation was found to be ca. 42% at 100% of the cellulose conversion in the presence of Ru@Fe$_3$O$_4$/HPS.

**Keywords:** cellulose; hydrogenolysis; magnetic catalyst; hyper-cross-linked polystyrene; glycols; mathematical modeling; reaction kinetics

## 1. Introduction

Being the most abundant component of lignocellulose biomass, cellulose plays a vital role not only in the utilizing of renewable resources, but also in providing additional opportunities for the production of different molecules-platforms through catalytic processes such as hydrogenolysis, oxidation, or selective reduction [1–3]. Glycols are the most important raw materials for many branches of modern industry. Ethylene glycol (EG) and propylene glycol (PG) are used in large volumes for the production of medicinal substances, surfactants, antifreeze, lubricants, solvents, fuels, and synthesis of polyester fibers and resins [4,5]. The question of how to effectively catalyze the conversion of cellulose into desired products is an interesting subject for many researchers. EG and PG can be obtained under one-pot conditions by hydrogenolysis of cellulose or polyols in the presence of heterogeneous catalysts [1,6–8]. In the processes of hydrogenolysis of cellulose to glycols, Ru-containing catalytic systems are considered to be active catalysts [9–13].

Magnetically recoverable catalysts have received considerable attention in the last decade due to the possibility of magnetic separation, which makes it easy to recovery with minimal catalyst losses. In addition, this leads to energy savings and a catalyst made of rare metals and leads to cheaper target products [14]. For the processing of lignocellulose

biomass magnetically recoverable catalysts are found in such processes as (i) the transformation of carbohydrates or carbohydrate-derived chemicals into valuable chemicals and liquid fuels [15], and (ii) conversion of cellulose into high yields of reducing sugar [16]. For instance, heterogeneous Pd-Fe catalysts may be successfully used in important sustainable reactions including the selective C-C and C-O bond cleavage of (i) $C_2$–$C_6$ polyols; (ii) furfurals; and (iii) phenol derivatives. For example, heterogeneous Pd-Fe catalysts can be successfully used in important stable reactions, including selective cleavage of C-C and C-O bonds (i) $C_2$–$C_6$ polyols; (ii) furfurals; (iii) phenol derivatives; and (iv) aromatic esters in the presence of molecular $H_2$ [17].

As a rule, inorganic materials such as carbon composites and inorganic oxides are utilized as catalyst supports [18]. At the same time, polymer materials, which are successful carriers for the formation of catalytically active nanoparticles, attract much attention from researchers [19]. In the review [20], for many organic synthesis processes, the authors noted the high catalytic activity of ruthenium nanoparticles stabilized with polyvinylpyrrolidone (PVP). Unfortunately, the thermal instability of PVP does not allow the use of such catalysts for high-temperature processes. Hyper-cross-linked polystyrene (HPS) is one of the first examples of the use of thermally stable polymer porous materials for the synthesis of catalytic systems by immobilization of noble metal nanoparticles (Pt, Pd, Ru, etc.). [19,21–23]. HPS is characterized by hierarchical porosity, which makes it possible to form a catalytically active metal-containing phase in the mesopores of the carrier and utilize it in organic synthesis processes. Authors [24] utilized Pd nanoparticles based on HPS in the selective hydrogenation of C-C triple bonds in alkynols. Au core–Pd shell bimetallic nanoparticles immobilized within HPS have been studied in the Suzuki cross-coupling [25]. In our early work, we synthesized ruthenium catalysts that showed high activity in the process of hydrolytic hydrogenation of cellulose to hexitols [26].

In the current study, the magnetically separable Ru-containing catalysts were synthesized for the first time using the polymeric matrix of hypercrosslinked polystyrene (HPS) as support. The structure and composition of the synthesized catalyst were studied by the physics-chemical methods (i.e., transmission electron microscopy, X-ray powder diffraction, X-ray photoelectron spectroscopy). The formation of magnetite nanoparticles ($Fe_3O_4$) with the following deposition of $RuO_2$ in the HPS pores was shown. The synthesized catalyst showed high activity in the hydrogenolysis of cellulose to form glycols and seemed to be stable at least in three consecutive cycles.

The experimental data obtained in the study of cellulose and glucose hydrogenolysis in the presence of the synthesized magnetically separable catalyst were used to propose the formal description of the process kinetics. The mathematical model of the reaction of glucose hydrogenolysis into EG and PG as a part of the catalytic cellulose conversion process into glycols was developed and the kinetic parameters were calculated.

## 2. Materials and Methods

### 2.1. Materials

HPS of the Macronet MN270 brand (Purolite Ltd., Llantrisant, UK) was utilized. It was washed with distilled water and acetone and dried under vacuum. Tetrahydrofuran (THF, ≥99.9%), ethanol (EtOH, ≥99.8%), methanol (MeOH, 99.5%), sodium hydroxide (NaOH, ≥98%), iron (III) chloride ($FeCl_3$, 97%), and sodium acetate ($CH_3COONa$ ≥ 99%) were obtained from Sigma-Aldrich. Ruthenium (IV) hydroxochloride (pure, OJSC Aurat, Moscow, Russia) was used as-received. All chemicals were used as-received. Distilled water was purified with an Elsi-Aqua water purification system.

### 2.2. Catalyst Synthesis

The dried HPS was powdered in a mill. For the synthesis of catalysts, a fraction with an average particle size of no more than 45 μm was used.

HPS-based magnetically recoverable Ru-containing catalysts were synthesized according to the following procedure. First, $Fe_3O_4$ particles were formed in the polymeric matrix

of HPS. In a typical experiment, 0.3 g of HPS was placed to the 10 mL of EtOH with preliminarily dissolved calculated amounts of $FeCl_3$ and $CH_3COONa$. After vigorous stirring, the sample of iron-containing HPS was dried at 70 °C, wetted with ethylene glycol, and placed in an autoclave reactor with Teflon coating. Then, the sample was heated up to 200 °C in argon medium and maintained at this temperature for 5 h. The resulting $Fe_3O_4$/HPS was washed with distilled water several times, and then again with EtOH, while being maintained by a magnet. A washed sample of magnetically separable $Fe_3O_4$/HPS containing ca. 20 wt.% of Fe was dried at 70 °C till constant weight was achieved.

For the synthesis of Ru@$Fe_3O_4$/HPS catalyst, $Fe_3O_4$/HPS was impregnated according to moisture absorption capacity with the solution of the calculated amount of ruthenium (IV) hydroxochloride in a complex solvent consisting of tetrahydrofuran, methanol, and water at a volume ratio 4:1:1 at room temperature. Further, the catalyst was dried at 70 °C, consecutively treated with solutions of NaOH and $H_2O_2$, and then washed with water until the absence of chloride anions in the washing water. The catalyst purified was dried at 85 °C. Then the catalyst was reduced in hydrogen flow (flow rate 100 mL/min) at 300 °C for 2 h, cooled in nitrogen, and kept under air.

In this way, a Ru-containing system containing magnetite particles with an estimated ruthenium content of 3 wt.% was synthesized. The results of X-ray fluorescence analysis (Zeiss AG, Jena, Germany) showed that the catalyst synthesis procedure provides final ruthenium content in the catalyst (2.7%). The average iron content is 19.6%.

### 2.3. Characterization

Electron-transparent specimens for transmission electron microscopy (TEM) were prepared by placing a drop of a sample suspension onto a carbon-coated Cu grid. Images were acquired at an accelerating voltage of 80 kV on a JEOL JEM1010 transmission electron microscope (JEOL, Pleasanton, CA, USA). Images were analyzed with the National Institute of Health developed image-processing package ImageJ (NIH) to estimate nanoparticle diameters.

X-ray powder diffraction (XRD, Malvern Panalytical, Malvern, UK) patterns were collected on an Empyrean from PANalytical. X-rays were generated from a copper target with a scattering wavelength of 1.54 Å. The step size of the experiment was 0.02.

Magnetic measurements were performed on a vibration magnetometer VIBRACh (TvSU, Tver, Russia).

X-ray photoelectron spectroscopy (XPS, ULVAC-PHI, Inc., Osaka, Japan) experiments were performed using PHI Versa Probe II instrument equipped with a monochromatic Al K(alpha) source. The X-ray power of 25 W at 15 kV was used for a 100 μm beam size. Nitrogen adsorption measurements were carried out at liquid nitrogen temperature on a surface analyzer Beckman Coulter SA 3100 (Coulter Corporation, Brea, CA, USA). Samples were degassed at 90 °C in a vacuum.

### 2.4. Catalyst TESTING Procedure and Product Analysis

Our tests were conducted in a 50-$cm^3$ high-pressure steel reactor (Parr Instruments, Moline, IL, USA) equipped with a PARR 4843 controller and a propeller stirrer. In a typical test, the cellulose, the catalyst, and 30 mL of distilled water were placed into the reactor. The reactor was triply purged with hydrogen at a pressure of 60 bars; heating and stirring ($\approx$100 rpm). Upon reaching the operational temperature, the speed of the stirrer was increased to 600 rpm. This time was considered to be the starting point of the test. After each test, the catalyst was separated using a neodymium magnet. The liquid phase of the catalyst was analyzed on an UltiMate 3000 liquid chromatograph (Dionex, Sunnyvale, CA, USA) equipped with a refractometric detector. Cellulose conversion was calculated using the formula $X = [(m_{c0} - m_c)/m_{c0}] \times 100\%$, where $m_c$ is the weight of the cellulose residue after the reaction and $m_{c0}$ is the initial weight of the cellulose. Selectivity was calculated with the formula $S = [m_{pr}/(m_{c0} - m_c)] \times 100\%$, where $m_{pr}$ is the weight of the product.

## 3. Results

### 3.1. Catalyst Characterization

The magnetic properties of the synthesized $Fe_3O_4$/HPS samples were studied. The magnetization curves are presented in Figure 1. The experimental samples were shown to have a high saturation magnetization (4.5 ± 0.1 emu/g, Figure 1). This value is significantly higher than the value obtained for the $Fe_3O_4$/$SiO_2$ synthesized in our previous studies $-0.8$ emu/g [27]. The magnetization curves no remanence or coercivity is observed, demonstrating superparamagnetic behavior which is characterized for magnetite. The superparamagnetic character of the synthesized support is optimal, since superparamagnets have a much higher magnetic susceptibility, but their remanent saturation magnetization in the absence of an external magnetic field is zero. Such catalysts do not interact with steel parts of equipment and can be completely recovered. A high value of saturation magnetization allows for fast magnetic separation of the catalyst after the reaction.
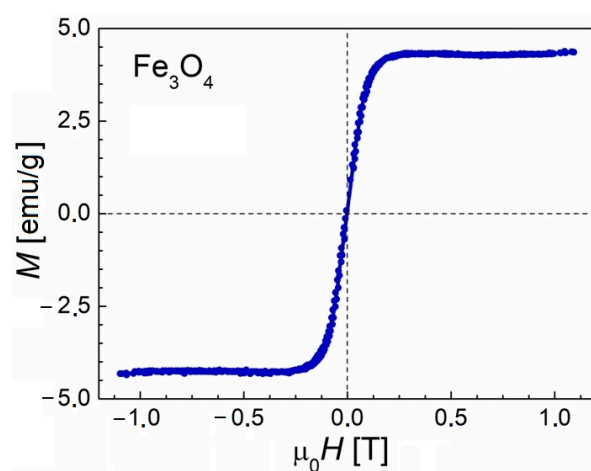


**Figure 1.** Isothermal magnetization curves of $Fe_3O_4$/HPS at 298 K.

Table 1 shows the porosity data of the initial HPS MN 270 and $Fe_3O_4$/HPS samples and the catalysts obtained from the nitrogen physisorption measurements.

**Table 1.** Porosity data for the initial HPS, $Fe_3O_4$/HPS, and the catalyst Ru@$Fe_3O_4$/HPS.

| Sample | $S_{BET}$, $m_2$/g | $S_L$, $m^2$/g | $S_t$, $m^2$/g | V, $cm^3$/g |
|---|---|---|---|---|
| HPS | 1075 | 1191 | 265 [1]; 807 [2]; 1072 | 0.37 |
| $Fe_3O_4$/HPS | 450 | 480 | 160 [1]; 289 [2]; 449 | 0.13 |
| Ru@$Fe_3O_4$/HPS | 364 | 392 | 175 [1]; 189 [2]; 364 | 0.08 |

SL is the specific surface area (Langmuir model); SBET is the specific surface area (BET model); St is the specific surface area (t-plot); V is the micropores volume; [1] specific surface area according to t-plot model; [2] specific surface area of micropores.

In our previous works, we showed that HPS has a hierarchical structure and contains about 40% of mesopores. Such structure is favorable for the formation of catalytically active nanoparticles in the polymer pores [22–26]. It was shown that with the formation of iron oxide and ruthenium-containing nanoparticles into the pores of the support, the specific surface area decreased from 1075 to 364 $m^2$/g (BET). The volume of micropores decreased from 0.37 to 0.08 $m^3$/g. It was assumed that the formation of magnetite particles occurs mainly on the surface of the HPS and in the mouths of the pores, which leads to their blockage and, consequently, a decrease in the specific surface area and a change in the ratio of micro-, meso-, and macropores of the samples.

The magnetite nature of the magnetic particles was also confirmed by powder X-ray diffraction. The XRD pattern of $Fe_3O_4$/HPS displays the sharper Bragg reflections whose intensity and positions are typical for those of magnetite (Figure 2a).
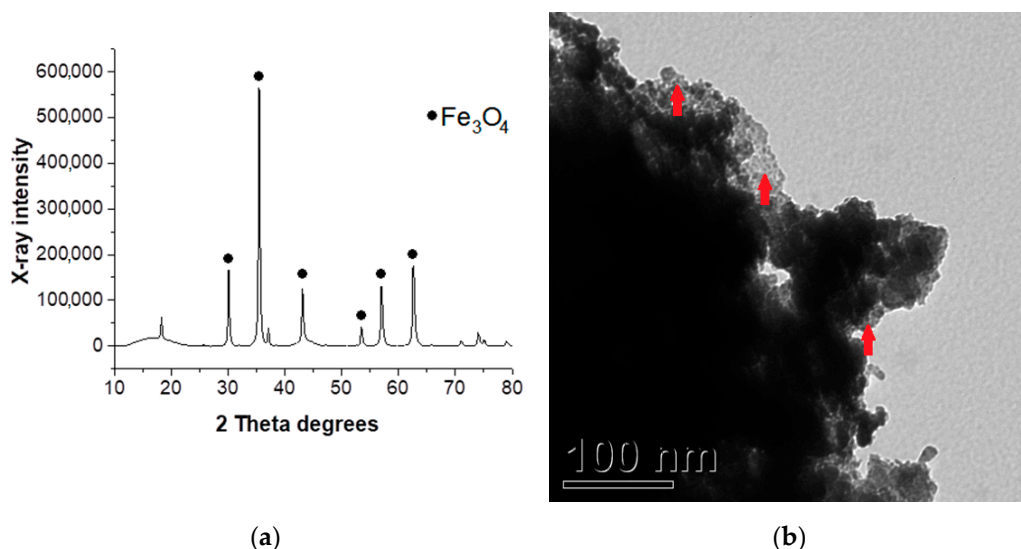
(**a**)  (**b**)

**Figure 2.** XRD pattern of the $Fe_3O_4$/HPS (**a**) and Ru-containing nanoparticles with mean diameter $2.0 \pm 0.5$ nm (**b**).

The average size of the magnetite and Ru-containing nanoparticles was determined by transmission electron microscopy. The mean magnetite nanoparticle diameter was $40 \pm 5$ nm. The mean Ru nanoparticle diameter was $2.0 \pm 0.5$ nm (Figure 2b).

For the study of the elemental composition of the catalyst surface and the chemical state of the metal-containing phases, the characterization of the Ru@$Fe_3O_4$/HPS was performed by the X-Ray photoelectron spectroscopy. The analysis of the survey spectra (Figure 3a) showed that the catalyst surface contains the atoms of C, O, Fe, Ru, N, and Cl. Table 2 presents the elemental composition of the Ru@$Fe_3O_4$/HPS surface. The mathematical modeling of the high-resolution spectra of Ru 3d and C 1s (Figure 3b) demonstrates that surface Ru species consist of the hydrated $RuO_2$ forms, while C is presented by the arene and alkane fragments of the polymeric matrix (284.8 eV) and carboxylic groups (289.2 eV). The modeling of Fe 2p high-resolution spectra confirmed that Fe on the surface belonged to $Fe_3O_4$.
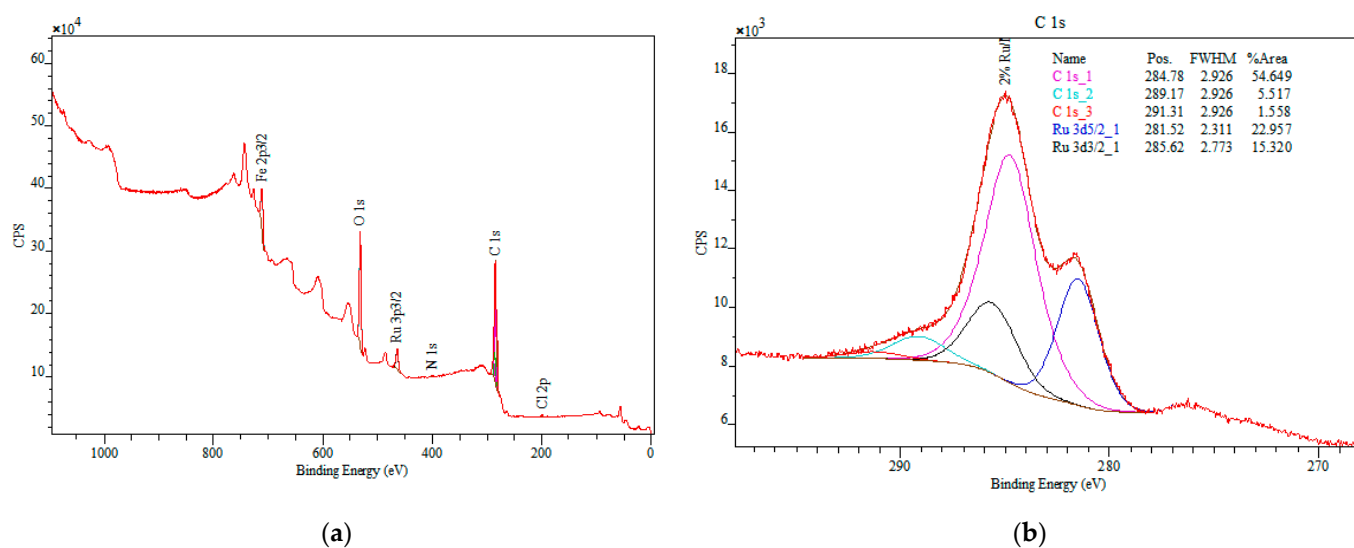


(**a**)  (**b**)

**Figure 3.** XPS survey (**a**), high-resolution spectra, and modeling of Ru 3d and C 1s (**b**).

**Table 2.** Surface element composition according to XPS.

| Element | C 1s | O 1s | N 1s | Cl 2p | Ru 3p$_{3/2}$ | Fe 2p$_{3/2}$ |
|---|---|---|---|---|---|---|
| %at/%wt. | 66.8/45.5 | 25.8/23.5 | 0.2/0.2 | 0.4/0.8 | 3.3/18.9 | 3.5/11.1 |

### 3.2. Cellulose Hydrogenolysis

Testing of the catalyst was carried out in the same conditions as in the previous study [27]: 255 °C, hydrogen partial pressure 60 bar, 50 min, 0.3 g of microcrystalline cellulose (a fraction with 0.045–0.063 μm particles size), 0.07 g of Ru@Fe$_3$O$_4$/HPS catalyst, 30 mL of H$_2$O, 0.195 mol of Ca(OH)$_2$ per 1 mol of cellulose. Under said experimental conditions, the maximum selectivity for PG and EG was 20.0% and 22.6%, respectively. Cellulose conversion in all runs was 100%. For comparison, two other catalysts have been tested as well: 5% Ru-Fe$_3$O$_4$/SiO$_2$ and 3% Ru/HPS developed by some of us [26]. The data in Table 3 show that the selectivity of Ru@Fe$_3$O$_4$/HPS catalyst was approximately equaled to the selectivity of the magnetically recoverable 5 % Ru-Fe$_3$O$_4$/SiO$_2$ catalyst, which earlier showed good results in the hydrogenolysis of cellulose to glycols [27]. However, due to the lower percentage of ruthenium in the new catalyst, its specific activity was higher by approximately 35% for EG and 20% for PG.

**Table 3.** Catalytic activities for EG and PG with the catalysts tested.

| Catalyst | Selectivity, % | | Specific Catalytic Activity Calculated as a Gram of EG or PG per Gram of Ru per Hour, h$^{-1}$ | |
|---|---|---|---|---|
| | EG | PG | EG | PG |
| Ru@Fe$_3$O$_4$/HPS | 22.6 | 20.0 | 39.12 | 34.62 |
| 5% Ru-Fe$_3$O$_4$/SiO$_2$ | 19.1 | 20.9 | 25.29 | 27.72 |
| 3% Ru/HPS | 7.4 | 12.5 | 7.51 | 12.71 |

255 °C; 60 bar H$_2$; 50 min; 0.3 g of cellulose; 0.07 g of catalyst; 30 mL H$_2$O; 0.195 mol of Ca(OH)$_2$ per 1 mol of cellulose.

The selectivity and activity values for the Ru/HPS catalyst turned out to be significantly lower, which can be explained by the absence of iron oxide in its composition, which has a promoting effect on the hydrogenolysis reaction [17]. In addition, it was reported by us [27] that when the catalytic nanoparticles (NPs) are deposited on iron oxide, the activities and selectivities in catalytic hydrogenolysis are significantly improved. Moreover, even when catalytic NPs are not deposited on the surface of iron oxide NPs, the close proximity of both NPs can result in collisions, leading to interactions and electron transfer from the iron oxide NP surface to the Ru surface due to partial reduction, facilitating hydrogenation and hydrogenolysis.

To study the catalyst stability Ru@Fe$_3$O$_4$/HPS was separated from the reaction medium using a neodymium magnet and then added to a fresh portion of cellulose, distilled water, and Ca(OH)$_2$. The data presented in Figure 4 indicate that the EG and PG selectivities at 100% conversion (~22.6 and 20%, respectively) and the activity do not change, revealing that the catalyst is stable under hydrothermal conditions of the hydrogenolysis process.
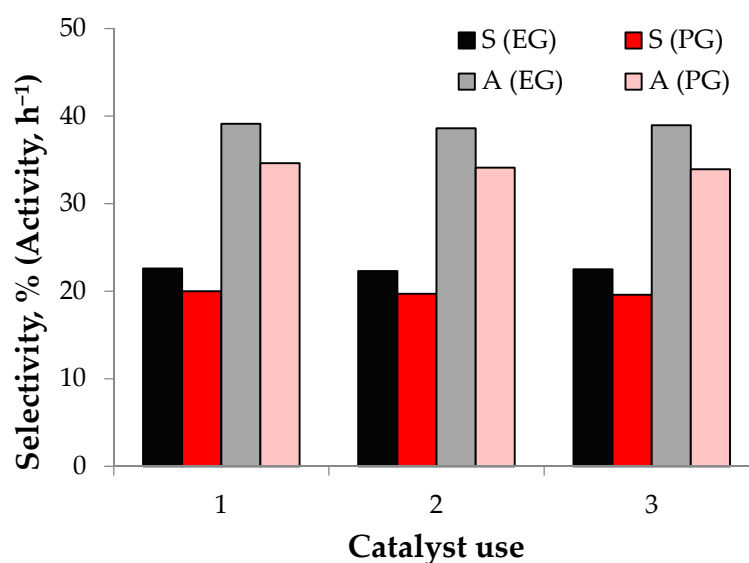
**Figure 4.** Selectivity (S) for glycols and specific catalytic activity (A) in the repeated use with Ru@Fe$_3$O$_4$/HPS (255 °C; 60 bar H$_2$; 50 min; 0.3 g of cellulose; 0.07 g of catalyst; 30 mL H$_2$O; 0.195 mol of Ca(OH)$_2$ per 1 mol of cellulose).

## 4. Discussion

There is a great number of studies devoted to the hydrolytic hydrogenation and hydrogenolysis of cellulose. However, only a small part of the investigations describes the kinetics of these processes, in particular, the formation of glycols. It can be associated with the number of reactions taking place simultaneously on the catalyst surface, i.e., hydrolysis, hydrogenation, retro aldol condensation, and epimerization [28]. The data obtained in this work allowed the mathematical modeling to be carried out and the formal kinetic model of the cellulose hydrogenolysis into glycols on the surface of Ru@Fe$_3$O$_4$/HPS catalyst to be proposed.

Cellulose hydrolysis at the temperatures of 250–260 °C proceeds fast. At the reaction conditions, the cellulose conversion degree reached up to 100% for 17–20 min of the process. On the other side, the presence of glucose in the reaction medium in this time range allowed the cellulose hydrogenolysis to be proposed as the limiting stage of the cellulose conversion process. Thus, the cellulose hydrolysis stage was excluded from the reaction pathway scheme presented below.

The main factor that determined the chemical behavior of the saccharine molecules, as well as the polyols, is the presence of a large number of hydroxyl groups. Because of the inductive effect, OH-groups lean the electronic density of C-C bonds. This results in the formation of a divisional positive charge which provides the facilitation of nucleophilic onset of the molecule and the C-C bond breaking. In this case, the central part of the molecule seems to be the most defenseless. Considering this, glucose and sorbitol hydrogenolysis can be proposed to proceed with the formation of C$_3$ compounds, in particular, glycerin and propylene glycol. These products were obtained in the reaction medium in high quantities. Hydrogenolysis of cellulose to ethylene and propylene glycol passes through several steps: cellulose hydrolysis, glucose hydrogenation, hydrogenolysis of C$_6$ compounds to C$_2$–C$_3$ fragments, etc. [29]. In the studied temperature range, glucose is hydrogenized fast forming sorbitol. At the initial stage of the reaction, the hexaols were found to be accumulated in high concentrations. Besides, a high amount of sorbitol in the reaction medium is determined by its higher stability at high temperatures in comparison with glucose. Opposed to glucose, the sorbitol molecule does not contain σ,π-coupling caused by the enolization and leading to the C-C bond weakening.

To choose an adequate kinetic model fitting the experimental data, different ways of the glucose hydrogenolysis to glycols were analyzed and the following reaction scheme was proposed (Figure 5).
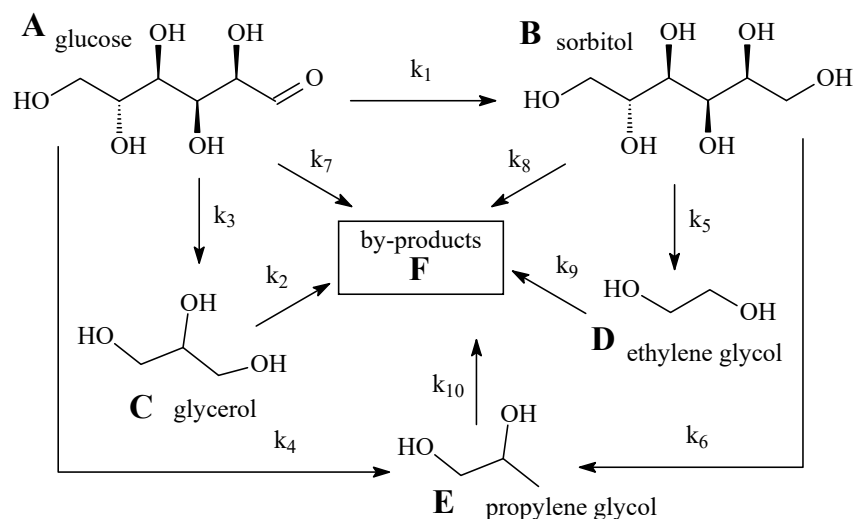


**Figure 5.** The scheme of glucose hydrogenolysis into glycols in the presence of a Ru@Fe$_3$O$_4$/HPS magnetic catalyst.

According to the theory [30,31], the rate of a heterogeneous catalytic reaction in the kinetic region is in proportion to the load on the catalyst $q = C_0/C_{cat.}$, where $C_0$—substrate concentration in the reaction mixture, $C_{cat.}$—catalyst concentration in the reaction mixture. The experiments showed the linear dependence of the glucose half-life ($\tau_{0.5}$) on the load on the catalyst similar to the dependence $\ln(\tau_{0.5})$—$\ln(q)$, as can be seen in Figure 6. In this case, it is suitable to use a reduced time parameter $\theta$ for the kinetic modeling. This parameter can be stated as $\theta = \tau/q$, where $\tau$—reaction time.
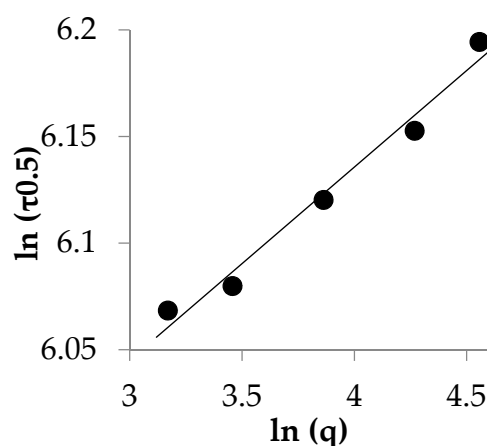


**Figure 6.** Dependence of $\ln(\tau_{0.5})$ on $\ln(q)$ for glucose hydrogenolysis in the presence of Ru@Fe$_3$O$_4$/HPS.

To generalize the experimental data obtained at different values of load on the catalyst (q), a switch to the numerical concentration of glucose and hydrogenolysis products was carried out as $X_i = C_i/C_0$, where $C_i$—product current concentration, mol/L; $C_0$—glucose current concentration, mol/L. The experimental data were scaled to the coordinates $X{\sim}\theta$.

Thus, the mathematic modeling of the experimental data can be presented as a system of differential equations:

$$(dX_A/d\theta) = -k_1[A] - k_3[A] - k_4[A] - k_7[A]$$

$$(dX_B/d\theta) = k_1[A] - k_5[B] - k_6[B] - k_8[B]$$

$$(dX_C/d\theta) = k_3[A] - k_2[C]$$

$$(dX_D/d\theta) = k_5[B] - k_9[D]$$

$$(dX_E/d\theta) = k_4[A] + k_6[B] - k_{10}[E]$$

$$(dX_F/d\theta) = k_7[A] + k_8[B] + k_2[C] + k_9[D] + k_{10}[E]$$

where $(dX_i/d\theta)$—reaction rate at the initial substrate concentration $C_o = 1$ mol/L and the catalyst concentration $C_{cat.} = 1$ mol/L.

The inverse problem of the kinetics was solved by the decisive integral method using the software developed by the SB RAS Boreskov Institute of the Catalysis (Novosibirsk, Russia). The data calculated according to the model were compared with those obtained by the experiments. The value of the root–mean–square (RMS) deviation was used to choose the mathematic model fitting the experimental data (Figure 7).
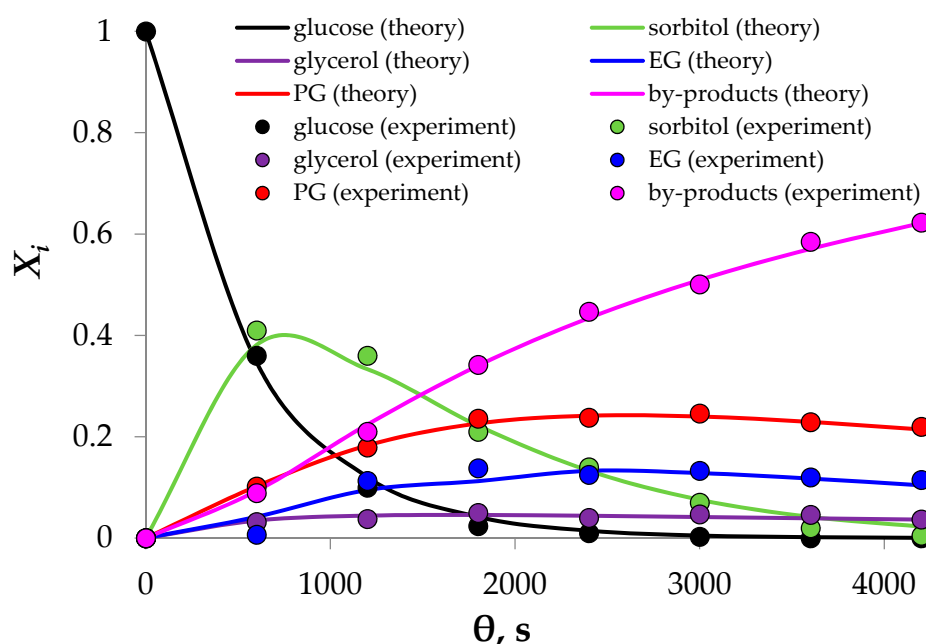


**Figure 7.** $X{\sim}\theta$ dependence for glucose hydrogenolysis over Ru@Fe$_3$O$_4$/HPS.

The rate constant values calculated for glucose hydrogenolysis according to the model are presented in Table 4.

**Table 4.** Kinetic parameters obtained according to the mathematic model of glucose hydrogenolysis.

| Parameter, $(mol/mol)_n \cdot s^{-1}$ | Value | Parameter, $(mol/mol)_n \cdot s^{-1}$ | Value |
|---|---|---|---|
| $k_1$ | $1.47 \pm 0.07 \times 10^{-3}$ | $k_6$ | $3.41 \pm 0.17 \times 10^{-4}$ |
| $k_2$ | $1.14 \pm 0.06 \times 10^{-4}$ | $k_7$ | $4.55 \pm 0.23 \times 10^{-5}$ |
| $k_3$ | $9.72 \pm 0.49 \times 10^{-5}$ | $k_8$ | $4.35 \pm 0.22 \times 10^{-4}$ |
| $k_4$ | $1.45 \pm 0.07 \times 10^{-4}$ | $k_9$ | $2.81 \pm 0.14 \times 10^{-4}$ |
| $k_5$ | $2.90 \pm 0.14 \times 10^{-4}$ | $k_{10}$ | $1.61 \pm 0.08 \times 10^{-4}$ |

The RMS deviation of the experimental data from the calculated: $1.30 \times 10^{-2}$.

The formal description obtained for the glucose hydrogenolysis over Ru@Fe$_3$O$_4$/HPS suggests the lack of adsorption or coordination interactions between the substrate or product molecules and the catalyst surface.

## 5. Conclusions

The synthesis method of catalyst (Ru@Fe$_3$O$_4$/HPS) was developed. Synthesized magnetically recoverable supports and catalysts were characterized by different physical-chemical methods. The use of this catalyst in the process of microcrystalline cellulose hydrogenolysis in subcritical water at 255 °C, 60 bar hydrogen pressure in 50 min allows PG and EG selectivities of 20.0 and 22.6%, respectively, at 100% of cellulose conversion. The catalyst is stable under hydrothermal conditions of the process; it is easily separated from the liquid phase with the external magnetic field and can be reused.

The magnetically separable catalyst stabilized in polymer pores is characterized by better magnetization in comparison with those deposited on SiO$_2$ synthesized in our previous works. This makes the catalyst to be more technologically advanced and convenient to use. Besides, the activity of the developed catalytic system in cellulose hydrogenolysis to EG and PG was found to be 35% and 20% higher compared to 5% Ru-Fe$_3$O$_4$/SiO$_2$ and much higher than those obtained over the HPS-supported catalyst without magnetite.

The formal description of the kinetics of glucose hydrogenolysis as one of the stages of cellulose conversion into glycols was obtained. The mathematic model of glucose hydrogenolysis to glycols in the presence of Ru@Fe$_3$O$_4$/HPS was proposed. The kinetic parameter estimation was performed according to the model developed.

The results obtained can be used for the development of the effective technology of natural polysaccharides conversion into chemicals and fuels.

**Author Contributions:** Conceptualization, O.M. and V.M.; methodology, Y.K. and O.M.; software, Y.K.; validation, O.K., and V.S.; formal analysis, A.B. and A.S.; investigation, O.M., O.K.; resources, M.S.; data curation, Y.K.; writing—original draft preparation, O.M. and V.M.; writing—review and editing, O.M., V.M. and M.S.; visualization, O.M.; supervision, O.K.; project administration, M.S.; funding acquisition, M.S. All authors have read and agreed to the published version of the manuscript.

**Conflicts of Interest:** The authors declare no conflict of interest.

## References

1. Xin, H.; Hu, X.; Cai, C.; Wang, H.; Zhu, C.; Li, S.; Xiu, Z.; Zhang, X.; Liu, Q.; Ma, L. Catalytic Production of Oxygenated and Hydrocarbon Chemicals From Cellulose Hydrogenolysis in Aqueous Phase. *Front. Chem.* **2020**, *8*, 146. [CrossRef]
2. Cai, C.; Wang, H.; Xin, H.; Zhu, C.; Zhang, Q.; Zhang, X.; Wang, C.; Liu, Q.; Ma, L. Hydrogenolysis of biomass-derived sorbitol over La-promoted Ni/ZrO$_2$ catalysts. *RSC Adv.* **2020**, *10*, 3993. [CrossRef]
3. Godina, L.I.; Kirilin, A.V.; Tokarev, A.V.; Simakova, I.L.; Murzin, D.Y. Sibunit-Supported Mono- and Bimetallic Catalysts Used in Aqueous-Phase Reforming of Xylitol. *Ind. Eng. Chem. Res.* **2018**, *57*, 2050–2067. [CrossRef]
4. Mounguengui-Diallo, M.; Sadier, A.; Noly, E.; Da Silva Perez, D.; Pinel, C.; Perret, N.; Besson, M. C-O Bond Hydrogenolysis of Aqueous Mixtures of Sugar Polyols and Sugars over ReO$_x$-Rh/ZrO$_2$ Catalyst: Application to an Hemicelluloses Extracted Liquor. *Catalysts* **2019**, *9*, 740. [CrossRef]
5. Yue, H.; Zhao, Y.; Ma, X.; Gong, J. Ethylene glycol: Properties, synthesis, and applications. *Chem. Soc. Rev.* **2012**, *41*, 4218–4244. [CrossRef]
6. Zheng, M.; Pang, J.; Sun, R.; Wang, A.; Zhang, T. Selectivity Control for Cellulose to Diols: Dancing on Eggs. *ACS Catal.* **2017**, *7*, 1939–1954. [CrossRef]
7. Gu, M.; Shen, Z.; Yang, L.; Dong, W.; Kong, L.; Zhang, W.; Peng, B.-Y.; Zhang, Y. Reaction Route Selection for Cellulose Hydrogenolysis into C$_2$/C$_3$ Glycols by ZnO-Modified Ni-W/β-zeolite Catalysts. *Sci. Rep.* **2019**, *9*, 11938. [CrossRef]
8. te Molder, T.D.J.; Kersten, S.R.A.; Lange, J.P.; Ruiz, M.P. Ethylene Glycol from Lignocellulosic Biomass: Impact of Lignin on Catalytic Hydrogenolysis. *Ind. Eng. Chem. Res.* **2021**, *60*, 7043–7049. [CrossRef]

9. Ribeiro, L.S.; Orfao, J.J.M.; Pereira, M.F.R. Insights into the effect of the catalytic functions on selective production of ethylene glycol from lignocellulosic biomass over carbon supported ruthenium and tungsten catalysts. *Bioresour. Technol.* **2018**, *263*, 402–409. [CrossRef]

10. Seretis, A.; Diamantopoulou, P.; Thanou, I.; Tzevelekidis, P.; Fakas, C.; Lilas, P.; Papadogianakis, G. Recent Advances in Ruthenium-Catalyzed Hydrogenation Reactions of Renewable Biomass-Derived Levulinic Acid in Aqueous Media. *Front. Chem.* **2020**, *8*, 221. [CrossRef]

11. Guo, X.; Guan, J.; Li, B.; Wang, X.; Mu, X.; Liu, H. Conversion of biomass-derived sorbitol to glycols over carbon materials supported Ru-based catalysts. *Sci. Rep.* **2015**, *5*, 16451–16460. [CrossRef] [PubMed]

12. Zhou, J.; Liu, G.; Sui, Z.; Zhou, X.; Yuan, W. Hydrogenolysis of sorbitol to glycols over carbon nanofibers- supported ruthenium catalyst: The role of base promoter. *Chin. J. Catal.* **2014**, *35*, 692–702. [CrossRef]

13. Pang, J.; Zhang, B.; Jiang, Y.; Zhao, Y.; Li, C.; Zheng, M.; Zhang, T. Complete conversion of lignocellulosic biomass to mixed organic acids and ethylene glycol *via* cascade steps. *Green Chem.* **2021**, *23*, 2427–2436. [CrossRef]

14. Shifrina, Z.B.; Bronstein, L.M. Magnetically Recoverable Catalysts: Beyond Magnetic Separation. *Front. Chem.* **2018**, *6*, 298. [CrossRef]

15. Liu, B.; Zhang, Z. Catalytic Conversion of Biomass into Chemicals and Fuels over Magnetic Catalysts. *ACS Catal.* **2016**, *6*, 326–338. [CrossRef]

16. Li, X.; Li, X.; Qi, W.; Shi, J.; Zhang, J.; Xu, Y.; Pang, J. Preparation of magnetic biomass-based solid acid catalyst and effective catalytic conversion of cellulose into high yields of reducing sugar. *BioRes* **2015**, *10*, 6720–6729. [CrossRef]

17. Espro, C.; Gumina, B.; Paone, E.; Mauriello, F. Upgrading Lignocellulosic Biomasses: Hydrogenolysis of Platform Derived Molecules Promoted by Heterogeneous Pd-Fe Catalysts. *Catalysts* **2017**, *7*, 78. [CrossRef]

18. García-Sancho, C.; Luque, R. Editorial Catalysts: Special Issue on Heterogeneous Catalysis for Valorization of Lignocellulosic Biomass. *Catalysts* **2021**, *11*, 649. [CrossRef]

19. Shifrina, Z.B.; Matveeva, V.G.; Bronstein, L.M. Role of Polymer Structures in Catalysis by Transition Metal and Metal Oxide Nanoparticle Composites. *Chem. Rev.* **2020**, *120*, 1350–1396. [CrossRef]

20. Axet, M.R.; Philippot, K. Catalysis with Colloidal Ruthenium Nanoparticles. *Chem. Rev. Am. Chem. Soc.* **2020**, *120*, 1085–1145. [CrossRef] [PubMed]

21. Tan, L.; Tan, B. Hypercrosslinked porous polymer materials: Design, synthesis, and applications. *Chem. Soc. Rev.* **2017**, *46*, 3322. [CrossRef] [PubMed]

22. Sidorov, S.N.; Volkov, I.V.; Davankov, V.A.; Tsyurupa, M.P.; Valetsky, P.M.; Bronstein, L.M.; Karlinsey, R.; Zwanziger, J.W.; Matveeva, V.G.; Sulman, E.M.; et al. Platinum-Containing Hyper-Cross-Linked Polystyrene as a Modifier-Free Selective Catalyst for L-Sorbose Oxidation. *J. Am. Chem. Soc.* **2001**, *123*, 10502–10510. [CrossRef]

23. Bronstein, L.M.; Goerigk, G.; Kostylev, M.; Pink, M.; Khotina, I.A.; Valetsky, P.M.; Matveeva, V.G.; Sulman, E.M.; Sulman, M.G.; Bykov, A.V.; et al. Structure and Catalytic Properties of Pt-Modified Hyper-Cross-Linked Polystyrene Exhibiting Hierarchical Porosity. *J. Phys. Chem. B* **2004**, *108*, 18234–18242. [CrossRef]

24. Nikoshvili, L.Z.; Bykov, A.V.; Khudyakova, T.E.; LaGrange, T.; Heroguel, F.; Luterbacher, J.S.; Matveeva, V.G.; Sulman, E.M.; Dyson, P.J.; Kiwi-Minsker, L. Promotion Effect of Alkali Metal Hydroxides on Polymer-Stabilized Pd Nanoparticles for Selective Hydrogenation of C-C Triple Bonds in Alkynols. *Ind. Eng. Chem. Res.* **2017**, *56*, 13219–13227. [CrossRef]

25. Nemygina, N.A.; Nikoshvili, L.Z.; Tiamina, I.Y.; Bykov, A.V.; Smirnov, I.S.; LaGrange, T.; Kaszkur, Z.; Matveeva, V.G.; Sulman, E.M.; Kiwi-Minsker, L. Au Core-Pd Shell Bimetallic Nanoparticles Immobilized within Hyper-Cross-Linked Polystyrene for Mechanistic Study of Suzuki Cross-Coupling: Homogeneous or Heterogeneous Catalysis? *Org. Process Res. Dev.* **2018**, *22*, 1606–1613. [CrossRef]

26. Matveeva, V.G.; Sulman, E.M.; Manaenkov, O.V.; Filatova, A.E.; Kislitza, O.V.; Sidorov, A.I.; Doluda, V.Y.; Sulman, M.G.; Rebrov, E.V. Hydrolytic Hydrogenation of Cellulose in Subcritical Water with the Use of the Ru-Containing Polymeric Catalysts. *Catal. Today* **2017**, *280*, 45–50. [CrossRef]

27. Manaenkov, O.; Mann, J.; Kislitza, O.; Losovyj, Y.; Stein, B.; Morgan, D.; Pink, M.; Lependina, O.; Shifrina, Z.; Matveeva, V.; et al. Ru-containing Magnetically Recoverable Catalysts: A Sustainable Pathway from Cellulose to Ethylene and Propylene Glycols. *ACS Appl. Mater. Interfaces* **2016**, *8*, 21285–21293. [CrossRef]

28. Schlaf, M.; Zhang, Z.C. Reaction Pathways and Mechanisms in Thermocatalytic Biomass Conversion I. In *Mechanism and Kinetic Analysis of the Hydrogenolysis of Cellulose to Polyols*; Chapter 9; Springer: Singapore, 2016; pp. 227–260. [CrossRef]

29. Tajvidi, K.; Hausoul, P.J.C.; Palkovits, R. Hydrogenolysis of Cellulose over Cu-Based Catalysts—Analysis of the Reaction Network. *ChemSusChem* **2014**, *7*, 1311–1317. [CrossRef] [PubMed]

30. Schlögl, R. Heterogeneous Catalysis. *Angew. Chem. Int. Ed.* **2015**, *54*, 3465–3520. [CrossRef]

31. Barbato, M.; Bruno, C. Heterogeneous Catalysis: Theory, Models and Applications. *Mol. Phys. Hypersonic Flows* **1996**, 139–160. [CrossRef]